

# Visualization and analysis of apolipoprotein A-I interaction with binary phospholipid bilayers

M. Alejandra Tricerri,<sup>1,\*</sup> Juan D. Toledo,<sup>\*</sup> Susana A. Sanchez,<sup>†</sup> Theodore L. Hazlett,<sup>†</sup> Enrico Gratton,<sup>†</sup> Ana Jonas,<sup>§</sup> and Horacio A. Garda<sup>\*</sup>

Instituto de Investigaciones Bioquímicas,<sup>\*</sup> Consejo Nacional de Investigaciones Científicas y Tecnológicas-Universidad Nacional de La Plata, La Plata, Argentina, 1900; Laboratory for Fluorescence Dynamics<sup>†</sup> and Department of Biochemistry,<sup>§</sup> University of Illinois at Urbana-Champaign, Urbana, IL 61801

**Abstract** Apolipoprotein A-I (apoA-I) interaction with specific cell lipid domains was suggested to trigger cholesterol and phospholipid efflux. We analyzed here apoA-I interaction with dimyristoylphosphatidylcholine/distearoylphosphatidylcholine (DMPC/DSPC) bilayers at a temperature showing phase coexistence. Solid and liquid-crystalline domains were visualized by two-photon fluorescence microscopy on giant unilamellar vesicles (GUVs) labeled with 6-dodecanoyl-2-dimethyl-amino-naphthalene (Laurdan). A decrease of vesicle size was detected as long as they were incubated with lipid-free apoA-I, together with a shape deformation and a relative enrichment in DSPC. Selective lipid removal mediated by apoA-I from different domains was followed in real time by changes in the Laurdan generalized polarization. The data show a selective interaction of apoA-I with liquid-crystalline domains, from which it removes lipids, at a molar ratio similar to the domain compositions. Next, apoA-I was incubated with DMPC/DSPC small unilamellar vesicles, and products were isolated and quantified. Protein solubilized both lipids but formed complexes relatively enriched in the liquid component. We also show changes in the GUV morphology when cooling down. Our results suggest that the most efficient reaction between apoA-I and DMPC/DSPC occurs in particular bilayer conditions, probably when small fluid domains are nucleated within a continuous gel phase and interfacial packing defects are maximal.—Tricerri, M. A., J. D. Toledo, S. A. Sanchez, T. L. Hazlett, E. Gratton, A. Jonas, and H. A. Garda. **Visualization and analysis of apolipoprotein A-I interaction with binary phospholipid bilayers.** *J. Lipid Res.* 2005. 46: 669–678.

**Supplementary key words** giant unilamellar vesicles • small unilamellar vesicles • lipid-protein interactions • lipid-phase coexistence

The factors underlying the protective capabilities of human HDL against atherogenesis have been extensively reviewed and supported by epidemiological studies and basic research. The correlation between high circulating levels

of HDL and a lower risk of cardiovascular disease was detected almost 30 years ago (1) and is still a topic of recent reports (2–4). Apolipoprotein A-I (apoA-I), the main protein component of HDL, participates in many of the metabolic steps of the HDL transformation. Some protective capabilities, including anti-inflammatory (5) and antioxidant properties (6) and removal of cytotoxic cholesterol from cell membranes (7), have been addressed, but especially its role in reverse cholesterol transport is considered critical (8). Many of the steps involved in cholesterol removal are likely to be mediated by apoA-I interactions with proteins at the cell surface. It is well known that ABCA1 facilitates the efflux of phospholipids (PLs), mostly phosphatidylcholine (PC), toward nascent apolipoproteins, which can then accept cholesterol, triggering the maturation and formation of HDL (9). Mature HDL, on the other hand, binds to scavenger receptor class B type I receptor, promoting free cholesterol efflux (10). Although binding of apoA-I to the cell surface is undoubtedly involved, it is not clear whether the interaction is direct with protein receptors or with adjacent membrane PLs (11, 12). Likewise, the relative contributions of distinct lipid domains at the plasma membrane, as rafts and more fluid domains, to overall lipid efflux are not well known (13).

The molecular mechanisms involved in the interactions of apoA-I with membranes are likely to require a significant degree of conformational and structural plasticity of the protein to adapt its conformation to the lipid environment. In a previous work (14), we studied the ability of

Abbreviations: Å, angstrom; apoA-I, apolipoprotein A-I; DMPC, dimyristoylphosphatidylcholine; DPPC, dipalmitoylphosphatidylcholine; DSPC, distearoylphosphatidylcholine; GP, general polarization; GUV, giant unilamellar vesicle; Laurdan, 6-dodecanoyl-2-dimethyl-amino-naphthalene; MLV, multilamellar vesicle; PAGE, polyacrylamide gradient gel electrophoresis; PC, phosphatidylcholine; PL, phospholipid; POPC, 1-palmitoyl, 2-oleoylphosphatidylcholine; Pt, Platinum; SUV, small unilamellar vesicle; TSB, Tris salt buffer.

<sup>1</sup> To whom correspondence should be addressed.  
e-mail: aletricerri@yahoo.com

Manuscript received 9 September 2004 and in revised form 9 November 2004 and in re-revised form 23 December 2004.

Published, JLR Papers in Press, January 16, 2005.  
DOI 10.1194/jlr.M400340JLR200

different conformations of apoA-I to interact with homogeneous unilamellar liposomes of 1-palmitoyl, 2-oleoylphosphatidylcholine (POPC) in the liquid-crystalline state. We compared binding affinities and lipid solubilization capabilities of lipid-free apoA-I and two well-defined reconstituted discoidal complexes, analogous to naturally occurring pre- $\beta$ -HDL. We found that the smaller reconstituted discoidal complexes [78 angstrom ( $\text{\AA}$ ) diameter] were the most efficient to rearrange when incubated with excess lipids, forming larger particles with higher PL contents. On the other hand, the protein in the lipid-free state bound to vesicles with higher affinity than the reconstituted discoidal complex but was not effective at forming lipidated products (14).

After incubating apoA-I with bilayers made of pure PC, lipid solubilization was observed to occur only at the transition temperature ( $T_m$ ) of the PL (15, 16), at which lipid-phase coexistence exists. Some authors attribute this property to the so-called "defects" generated at the border where the domains interact and where topological changes occur. These defects would facilitate the interaction of the protein with the lipid surface, allowing the formation of lipid-protein complexes.

In this work, we analyzed apoA-I interactions with liposomes containing a well-defined binary composition at temperature conditions in which lateral heterogeneity exists. The phase transition of this lipid mixture has been previously studied (17, 18), and the nonideal mixing properties of the dimyristoylphosphatidylcholine/distearoylphosphatidylcholine (DMPC/DSPC) make this system a good model to analyze phase separation and domain formation. We observed, isolated, and quantified the product of apoA-I rearrangement into lipid complexes. Additionally, we set out to determine whether there is a preferential interaction of apoA-I with different domains, using two-photon microscopy and a system that allows us to discriminate, in real time, the kinetics of lipid removal from each separate domain coexisting at the lipid bilayer. It was previously observed that apoA-I interaction with DMPC/DSPC (1:1 molar ratio) multilamellar vesicles (MLVs) was maximum at  $\sim 28^\circ\text{C}$  and that the efficiency of the recombination decreases dramatically a few degrees below and above this temperature (19). By visualizing the dependence of the coexisting lipid domain morphology with the temperature, we discuss the probable reason for this phenomenon.

## MATERIALS AND METHODS

### Materials

ApoA-I was purified from human plasma (donated by the Banco de Sangre del Instituto de Hemoterapia de La Plata), as described previously (20, 21). Dipalmitoylphosphatidylcholine (DPPC), DMPC, DSPC, and ultrapure guanidine hydrochloride were purchased from Sigma Chemical Co. (St. Louis, MO). 6-Dodecanoyl-2-dimethylamino-naphthalene (Laurdan) was from Molecular Probes (Eugene, OR), and [ $^{14}\text{C}$ ]methanaldehyde was from Dupont New England Nuclear Products (Boston, MA). All other reagents were pro analysis grade.

### ApoA-I interaction with giant unilamellar vesicles

**Giant unilamellar vesicle preparation.** Giant unilamellar vesicles (GUVs) were obtained as reported previously (14, 22). Briefly, stock solutions of PLs (pure DMPC, pure DSPC, or a mixture with a 1:1 molar ratio of DMPC/DSPC) were prepared in chloroform at a concentration of 0.2 mg/ml. Lipids ( $\sim 2\ \mu\text{l}$ ) were added to each Platinum (Pt) wire of the experimental chamber, dried under  $\text{N}_2$ , and lyophilized for  $\sim 30$  min to remove any traces of the remaining solvent. The chamber was sealed with a cover slip and thermostated with a circulating-water bath. Immediately before connecting the Pt wires to a function generator (Hewlett-Packard, Santa Clara, CA), 1 mM previously warmed Tris buffer, pH 8.0, was added to the chamber at a temperature  $\sim 65^\circ\text{C}$ , as detected by a digital thermocouple (model 400B; Omega, Stamford, CT). A low-frequency alternating current field (frequency, 10 Hz; amplitude, 2 V) was applied to grow the vesicles by the electroformation method (23). When the vesicles were formed, as detected by a charge-coupled device color video camera (CCD-Iris; Sony) attached to the microscope, we added 1  $\mu\text{l}$  of Laurdan from a DMSO stock solution (Laurdan-to-lipid molar ratio of 1:100) and incubated with the GUVs for  $\sim 15$  min. Then, we turned off the alternating current field and proceeded with the temperature scan. Temperature was decreased at an approximate rate of  $5^\circ\text{C}$  every 15 min until  $28^\circ\text{C}$  was achieved.

**Two-photon excitation microscopy measurements.** The principle and equipment for two-photon excitation microscopy have been described previously (14, 22). Using this system, we take advantage of the sectioning effect of the two-photon fluorescence microscope to visualize the surface morphology of coexisting domains in giant vesicles together with the unique capability that permits the measurement of instant generalized polarization (GP) values to quantify the evolution of each domain in the real time of the experiment. We used a scanning two-photon dual-channel fluorescence microscope developed at the Laboratory for Fluorescence Dynamics. An Axiovert 35 inverted microscope (Zeiss) received the excitation light (780 nm) from a titanium-sapphire laser (Mira 900; Coherent, Palo Alto, CA) pumped by a frequency-doubled Nd/vanadate laser (Verdi; Coherent). We used a Zeiss 20 $\times$  LD-Achroplan air objective (0.4 numerical aperture). The laser was guided by a scanner (Cambridge Technology, Watertown, MA) to achieve beam scanning in both the  $x$  and  $y$  directions. The input signal from a frequency synthesizer (Hewlett-Packard) was used to control the scanning rate. For the GP measurements, the emission light was split into red and blue channels using a ChromaTechnology 470DCXR-BS dichroic beam splitter in the emission path. Interference filters, either an Ealing 490 or an Ealing 440 (Holliston, MA), were placed in the appropriate emission paths to further isolate the red and blue parts of the emission spectrum. Separate detectors were used for each channel to simultaneously collect the 490 and 440 nm emissions. Correction for the wavelength dependence of the emission detection system was accomplished through the comparison of known solutions [Laurdan in DMSO or Laurdan in DMPC vesicles at  $20^\circ\text{C}$  (22, 24)] taken on an ISS, Inc. (Urbana, IL), model PC1 steady-state fluorometer. The separate red and blue images were simultaneously collected and then recombined to form the GP image of the sample using the SimFCS program.

**Properties of Laurdan.** Among several fluorescence probes, the spectroscopic characteristics of Laurdan offer a number of advantages for the study of phase coexistence in lipid systems. Additionally, Laurdan has been used successfully in combination with the two-photon techniques for lipid-lipid (22, 24–26) and lipid-protein (14) interactions.

The naphthalene moiety of this probe possesses a dipole moment that increases upon excitation and may cause reorientation

of the solvent dipoles. The energy of the probe's excited state decreases upon solvent reorientation, which is reflected in a red shift of the emission spectrum that is highly sensitive to the polarity of the environment. When added to PLs, Laurdan emission originates entirely from probes within the PL environment, as a result of its low solubility and quantum yield in water (27). The probe at the bilayer remains tightly anchored by cooperative van der Waals interactions between the lauric acid tail of the probe and the lipid hydrocarbon chains, with its fluorescence moiety residing at the level of the PL glycerol backbone (28).

**Laurdan intensity imaging of GUVs.** After the GUVs were grown and using the charge-coupled device camera attached to the scope, it was possible to choose a target GUV and follow its behavior after any particular treatment. To obtain a fluorescent image, Laurdan was added to the chamber containing the GUVs and 15–25 min of equilibration time was allowed before the image was taken.

The transition dipole of Laurdan in PL bilayers is aligned parallel to the acyl chain of the PLs. When vesicles are excited with polarized light, a photoselection occurs in the plane of the excitation light (29). When illuminating with circular polarized light in the  $x$ - $y$  plane, strong excitation will occur where the molecules

are parallel to the excitation; the effect will be particularly stronger in the  $x$ - $y$  plane that passes through the center of the vesicle. If we observe the top or bottom regions of a spherical lipid vesicle, the photoselection will decrease; as a consequence, we will observe poorly illuminated areas. In addition, this effect will depend upon the state of the lipids. In the liquid-crystalline phase, because of the lipid mobility, it is not unusual to find some components of the transition dipole parallel to the excitation polarization. This case is illustrated in Fig. 1A, panel 1. The most dramatic loss of fluorescence will occur when the excitation dipoles are perpendicular to the excitation plane (i.e., when gel domains are situated at the top or bottom of the vesicles). Thus, bright areas show liquid-crystalline domains, whereas dark regions show lipids present in the gel state. Figure 1A, panels 2–4, show a GUV in conditions in which liquid-crystalline and solid domains coexist at the surface of the vesicle. It is worth mentioning that no effect of Laurdan was observed on the  $T_m$  of the lipid mixture (30) or on lipid domain formation (26).

**Laurdan generalized polarization and GP images.** Laurdan emission maximum depends upon the phase state of the PLs, being blue in the gel phase (maximum emission at  $\sim 440$  nm) and green in

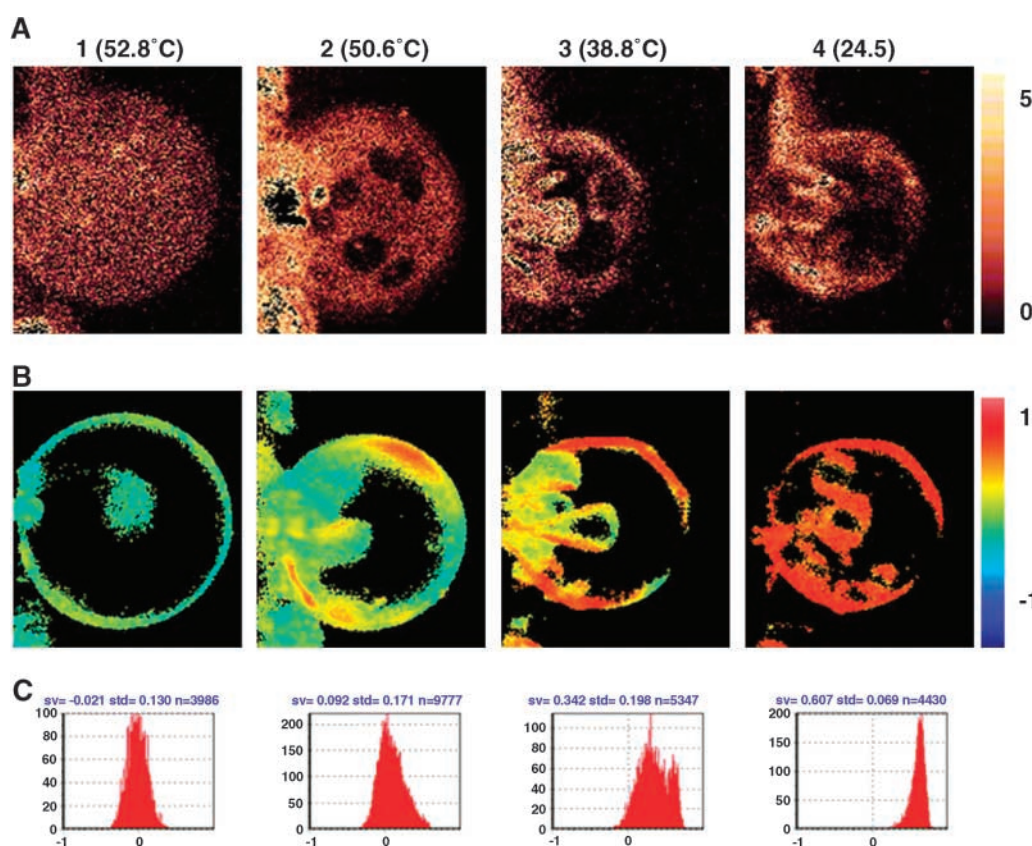


**Fig. 1.** Temperature dependence of the morphology of giant unilamellar vesicles (GUVs) containing dimyristoylphosphatidylcholine/distearoylphosphatidylcholine (DMPC/DSPC) at a molar ratio of 1:1. A: 6-Dodecanoyl-2-dimethyl-amino-naphthalene (Laurdan) images were taken on the surface of the GUV. At temperatures greater than  $\sim 50^\circ\text{C}$ , both lipids are in the liquid-crystalline state, and a homogenous bright area is observed (panel 1); panels 2 and 3 correspond to phase coexistence regions showing different domain shapes. Panel 4 shows the image of the GUV at a temperature condition in which both lipids are in the solid state. The image shows fluorescence intensity in a false color representation. B: Laurdan general polarization (GP) image taken at the center of the same GUV shown in a different color scale. C: GP histograms associated with the respective GP images. The coexistence of domains observed at the top of the GUVs (A, panels 2, 3) is correlated with the observation of different colors in the GP image in B and with a distorted GP histogram (same panels in C). GUVs were formed in 1 mM Tris buffer, pH 8.0.



the liquid-crystalline phase (maximum emission at  $\sim 490$  nm). To quantify the emission spectral changes, the GP function was defined as described (30):

$$GP = I_B - I_R/I_B + I_R \quad (\text{Eq. 1})$$

where  $I_B$  and  $I_R$  are the intensities in the blue and green edges of the emission spectrum, respectively. Thus, lower values of GP indicate an increased content or relaxation rate of water molecules surrounding Laurdan dipoles. In our two-photon microscope, a dual-channel setup was used and two simultaneous images were obtained, one for each region of the Laurdan spectrum. The two images were analyzed by the SimFCS program to obtain the GP image and the associated GP histogram (distribution of the GP values per pixel). To avoid deviations caused by vesicle curvature, GP distributions were obtained at the center of the vesicle. When the GUVs present a homogeneous distribution of GP (Fig. 1C, panels 1, 4), the GP histogram can be fitted with single Gaussian distribution, where the GP value at the center of the distribution corresponds to the average GP value. If two coexisting domains are observed in the GUV, the GP histogram clearly shows two components (Fig. 1C, panels 2, 3). If this is the case, the total GP (GPT) value is given by a sum of the fractional (fr) contribution of the pixels with different GP values:

$$GPT = GP_B \cdot fr_B + GP_G \cdot fr_G \quad (\text{Eq. 2})$$

where  $fr_B$  and  $fr_G$  are fractional contributions of the components with higher ( $GP_B$ ) and lower ( $GP_G$ ) GP values, extracted from the areas corresponding to each component in the distribution.

**Kinetics of the interaction of apoA-I with GUVs.** After vesicles were grown, they were kept at  $28^\circ\text{C}$  for  $\sim 30$  min to avoid any effect of temperature instability in the different measurements. To visualize morphological changes attributable to apoA-I interaction, we selected a vesicle and took single-channel images from the top at different times during 2 h after apoA-I addition. In a separate experiment, a vesicle was focused at the center and images scanned in both emission channels. Histograms were registered at different times, and GP and fractional evolutions were evaluated from the slopes of each curve using an ANOVA regression test.

As a control, to avoid any effect on the GP measurements caused by the protein binding to the bilayer, we incubated apoA-I with POPC GUVs and measured the GP before and after the addition of the protein. Under these conditions, lipid-free apoA-I binds to these vesicles without lipid solubilization, as we have demonstrated before (14). No change in GP was detected.

### ApoA-I interaction with small unilamellar vesicles

**Small unilamellar vesicle preparation.** Small unilamellar vesicles (SUVs), made of DMPC and DSPC, were prepared from stock solutions of the lipids in chloroform. Proper volumes were dried extensively under  $\text{N}_2$  and lyophilized for  $\sim 1$  h to remove any remaining traces of organic solvent. Tris salt buffer (TSB; 10 mM Tris, 150 mM NaCl, 0.01%  $\text{N}_3\text{Na}$ , and 0.01% EDTA, pH 8.0) was warmed to  $\sim 70^\circ\text{C}$  and added to the dried lipids to reach a 10 mg/ml PC concentration, vortexed, and sonicated under  $\text{N}_2$  until lipid dispersion became clear. Once SUVs were obtained, they were kept at a temperature above the  $T_m$  of the DMPC.

**Product size characterization.** To characterize the molecular size distribution of the products from the reaction between the DMPC/DSPC SUVs and the apoA-I, 10  $\mu\text{l}$  of apoA-I (4 mg/ml in TSB) was incubated with 10  $\mu\text{l}$  of 10 mg/ml liposomes (DMPC/DSPC 1:1 molar ratio) for 0, 0.5, 1, 3, 6, and 24 h at  $28^\circ\text{C}$ . Incubation was stopped by cooling down the samples on ice, and mixtures were analyzed by native polyacrylamide gradient gel electrophoresis (PAGGE) using an 8–25% gradient (Miniprotean II System; Phar-

macia). Product sizes were determined using high molecular weight markers (Amersham Biosciences), and protein was detected by Coomassie Blue stain (Bio-Rad).

**Protein and lipid determination.** In a separate experiment, a small amount of [ $^{14}\text{C}$ ]apoA-I, labeled as described (31), was added to the stock solution to achieve a specific activity of 3,000 cpm/ $\mu\text{g}$  protein. Radiolabeled protein was incubated with liposomes at  $28^\circ\text{C}$  at a weight ratio 2.5:1 PC to apoA-I. Aliquots of 500  $\mu\text{l}$  were taken at different times and fractionated with three columns in tandem (Superose 6 HR 10/30, Superdex 200 HR, and Superdex 75 from Pharmacia Biotech) pumped with a P-500 (Pharmacia Biotech). The elution profile was monitored by light absorbance at 280 nm (LKB Uvicord SII), and 700  $\mu\text{l}$  fractions were collected (LKB Bromma Fraction Collector and Recorder). Fractions corresponding to the remaining liposomes, lipid-protein complexes, and uncombined lipid-free apoA-I were pooled separately and concentrated to  $\sim 1$  ml into a SpeedVac System (Savant GMI). Samples were reanalyzed by PAGGE to confirm the expected molecular sizes and to ensure that no rearrangement had occurred during the concentration process.

Protein in aliquots of 200  $\mu\text{l}$  was quantified by scintillation counting (Rack-Beta), and 300  $\mu\text{l}$  of the remaining sample was used to quantify lipids as follows. A precise amount of multilamellar liposomes of DPPC was added to the sample after the concentration step and used as internal standard.

Lipids were extracted with chloroform-methanol (2:1) using the Folch procedure (32). Briefly, Folch mixture was added at 20% of the total volume, and partition was allowed to occur. The organic phase was extracted and concentrated under the vacuum achieved with a water pump. Borum trifluoride in methanol (Fluka) was added and heated for 3 h at  $65^\circ\text{C}$  to obtain the fatty acid methyl esters. Samples were analyzed by gas-liquid chromatography using a Hewlett-Packard HP 6890 apparatus (33).

**Light-scattering measurements.** SUVs (85  $\mu\text{g}$ ) containing a 1:1 molar ratio of DMPC/DSPC were added to 3 ml of TSB in a  $1 \times 1$  cm quartz cuvette and cooled down to  $10^\circ\text{C}$ . ApoA-I previously thermostated at the same temperature was added at a lipid-protein weight ratio of 2.5. After a few minutes at  $10^\circ\text{C}$ , temperature was modified as indicated (see Fig. 6). Light scattering was measured continuously in a SLM 4800 C spectrofluorometer (Champaign, IL) using excitation and emission wavelengths of 350 nm. Temperature was detected with a thermocouple immersed in the sample.

## RESULTS

### Characterization of the DMPC/DSPC GUVs

Vesicles were grown as described in Materials and Methods at  $65^\circ\text{C}$ . We followed the changes in morphology of the GUVs with the temperature. Intensity images were taken on the top of one target vesicle. This particular mixture has been partially characterized by members of the Laboratory for Fluorescence Dynamics (25), and a more detailed version is shown in Fig. 1. At  $\sim 65^\circ\text{C}$ , the DMPC/DSPC vesicles appeared as a bright round sphere; at this temperature, the two lipids are over their  $T_m$ , so both lipids are in the liquid state (Fig. 1A, panel 1). As soon as we decreased the temperature to less than  $\sim 55^\circ\text{C}$  (DSPC  $T_m$ ), some dark circular areas appeared, which were attributed to solid-state domains, rich in DSPC, coexisting with the liquid-crystalline DMPC-rich domains (Fig. 1A, panels 2, 3). As cooling continued, the shape of the do-

mains remained, but they moved around the vesicle, until the temperature reached  $\sim 37^\circ\text{C}$ . Then, a clear deformation of the round shape of the domains was observed (Fig. 1A, panel 3): many of the vesicles changed their morphology, losing their round shape, and some of them either detached from the Pt wires or collapsed.

To characterize the coexisting domains further, we focused the microscope at the center of the vesicles and acquired the GP image (see Materials and Methods) as a function of temperature (Fig. 1B). At  $65^\circ\text{C}$ , the observed homogeneous circumference of the lipid bilayer, labeled with Laurdan, corresponds with a homogeneous GP image (Fig. 1B, panel 1). As the temperature decreases, the dark areas appearing in the intensity image (Fig. 1A, panel 2) correspond with regions with a higher GP value in the center of the vesicle (Fig. 1B, panel 2), meaning two areas with different fluidity (Fig. 1B, panels 2, 3) (26). When  $\sim 24^\circ\text{C}$  is reached (Fig. 1B, panel 4), the system is again homogeneous but with a higher GP, corresponding to both lipids in the solid state. This behavior of the domains is in good agreement with previously reported phase diagrams (17, 18). With a 1:1 molar ratio, lateral phase separation should be expected between  $\sim 25^\circ\text{C}$  and  $50^\circ\text{C}$  for this system.

Figure 1C shows GP histograms that correspond to the distribution of GP values per pixel in the images. From the histograms, an average GP can be obtained. In the case of two coexisting phases, the histogram can be separated into two average GP values, one for each phase. **Figure 2** shows a detailed plot of the GP values obtained at different temperatures for GUVs made from the binary DMPC/DSPC mixture and also for GUVs made of pure DMPC or DSPC. As expected, the GP corresponding to

pure DSPC vesicles was higher than that corresponding to pure DMPC at the same temperature, and both GPs decreased abruptly around their corresponding  $T_m$  (i.e.,  $\sim 55^\circ\text{C}$  for DSPC and  $24^\circ\text{C}$  for DMPC). It should be expected that, if both lipids were completely mixed, the measured GP in the DMPC/DSPC GUVs should be the mean value of both lipids when they are pure in the vesicles. On the other hand, if lipids are not miscible, the solid domains should keep the GP values of the DSPC and the liquid domains should keep those of the pure DMPC. When we analyzed the GP distributions on each domain at the binary mixed GUVs, we found for gel-state domains GP values lower than for the pure DSPC (Fig. 2, open triangles). Instead, liquid domains showed GP values higher than the pure DMPC (Fig. 2, closed triangles). This fact agrees with previous observations by Leidy et al. (18) and corroborates a partial miscibility of the lipids in the vesicle.

### Interaction of apoA-I with DMPC/DSPC GUVs

The interaction of apoA-I with DMPC/DSPC GUVs was followed at  $28^\circ\text{C}$ . The Laurdan images at the top of the vesicle are shown in **Fig. 3**. As described above, at this temperature the vesicles are slightly collapsed, but the dark, round domains are still clear in the intensity images, as shown in Fig. 3, panel 1. Although a large heterogeneity is detected at the surface of the GUV, it is worth noting that, when vesicles lose their spherical shape because of the predominance of lipids in the solid state, the irregularity at the surface can result in the excitation of some dipoles that, even localized in solid environments, are not perpendicular to the excitation plane. Thus, a better estimation of phase and domain separation will be given by the GP image at the center of the vesicle, as shown in Fig. 1B. After the addition of apoA-I, a slight decrease in the size of the vesicle is observed (Fig. 3). As long as the incubation time increases, the bright areas corresponding to more liquid domains start to decrease and the dark areas (more solid domains) become predominant in the structure. At the same time, the vesicles lose their round shape. This indicates that the liquid component is preferentially being removed, and as a consequence the more rigid vesicle is not able to recover its spherical shape after removal of the liquid component. By moving up and down in the focal plane, we demonstrated that the decrease in vesicle size was not caused by movement of the vesicle out of the observation plane.

To further characterize the interaction of apoA-I with domains of different composition, we repeated the previous kinetics, but in this case after the evolution of the GP at the GUV center for 2 h. Fitting the distribution to a double Gaussian function, we calculated the average GP values (**Fig. 4A**) and fractional contributions of each domain (**Fig. 4B**) as described in Materials and Methods. The evolution of the fractions and GP with the incubation time is calculated from the slope of the regression line. The fraction of the liquid domains decreased [i.e., the fraction of the solid component increased as a function of the incubation time (**Fig. 4B**, closed squares)], confirming the previous observation that apoA-I removes lipids preferen-

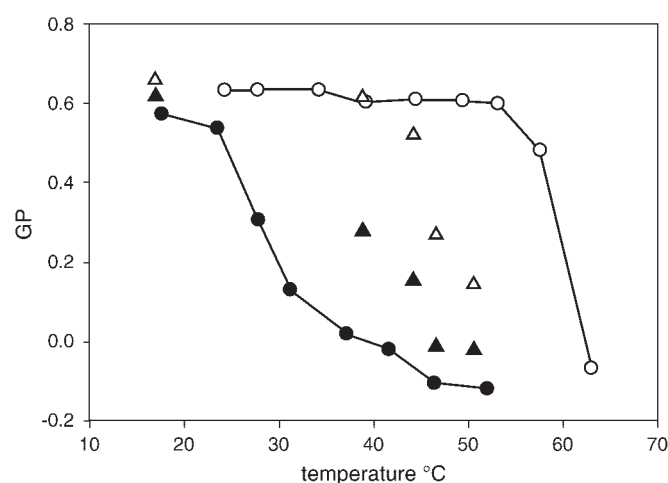


**Fig. 2.** Effect of temperature on the GP in DMPC (closed circles) and DSPC (open circles) pure vesicles and on the coexisting domains in vesicles containing equal amounts of both lipids. Each symbol represents the resulting GP value from fitting the histogram to a Gaussian distribution. The errors of the fittings are smaller than the symbol sizes ( $\sim 10^{-4}$ ). Open triangles represent the measured GP of the solid domains, and closed triangles represent the measured GP of the liquid-crystalline domains in the two-component vesicles.

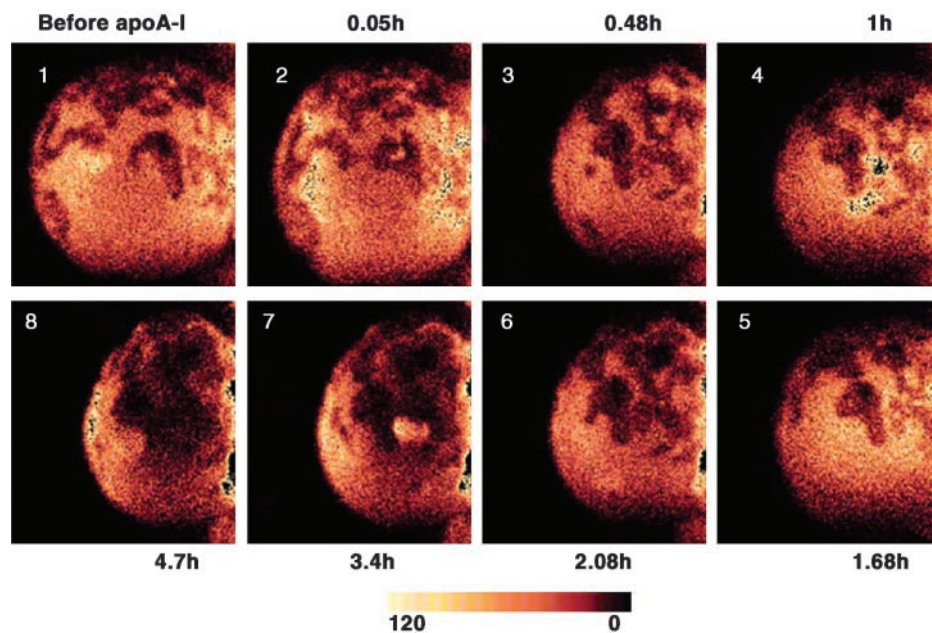


**Fig. 3.** Effect of apolipoprotein A-I (apoA-I) addition to DMPC/DSPC GUV morphology. Panel 1 shows the top of a Laurdan-doped vesicle after 30 min at 28°C, before apoA-I addition. The following panels show morphology changes of the same vesicle after incubation with apoA-I at the times indicated.

tially from the liquid phase. Instead, the average GP of each domain remained almost constant during the experiment, indicating that the composition of the domains did not vary significantly. This result indicates that protein extracts both lipids at a molar ratio similar to the composition present at the liquid domains before the addition of apoA-I.

According to the phase diagram previously reported by Mabrey and Sturtevant (17) for this mixture in MLV, starting with a DMPC/DSPC 1:1 molar ratio, the liquid phase at 28°C should contain a maximum of 10% DSPC. From the data shown in Fig. 2, the GP of pure DMPC at this tem-

perature is on the order of the values we obtained for liquid domains in the mixed vesicles (Fig. 4A, open circles), which is compatible with a small amount of DSPC present in these domains.

#### Interaction of apoA-I with DMPC/DSPC SUVs

To characterize the product of protein interaction with liposomes, we prepared SUVs containing equimolar amounts of DMPC and DSPC, incubated with apoA-I at 28°C for different times, and analyzed the product of the rearrangement by native PAGE (Fig. 5). We observed that for a very short time, protein interacted efficiently with SUVs,

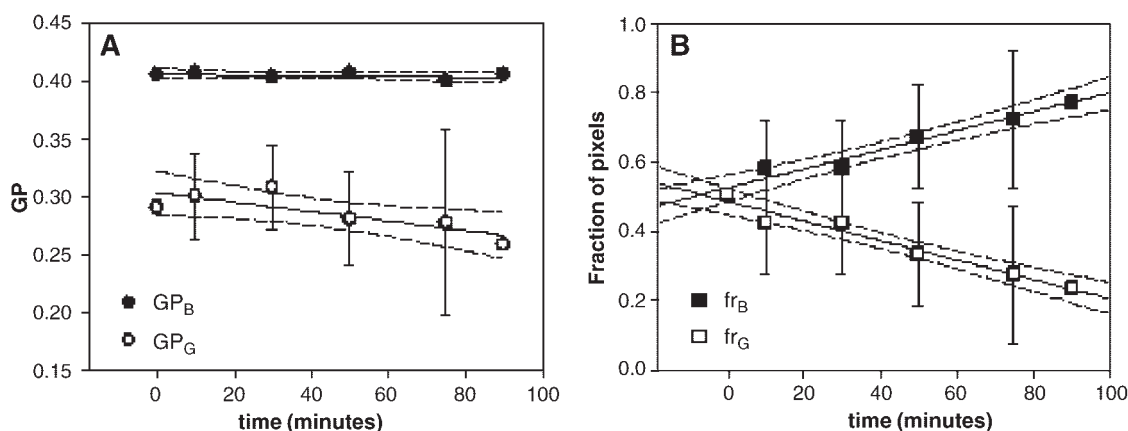


**Fig. 4.** Changes in GP values and fractional contributions after the addition of lipid-free apoA-I to 1:1 DMPC/DSPC GUVs at 28°C, calculated from the distribution as described above and defined by equation 2. A: Plot of GP as a function of time. Closed circles ( $GP_B$ ) correspond to the component in the gel state, and open circles ( $GP_G$ ) correspond to the lipids in the liquid-crystalline state. B: Time dependence of the fractional contributions for  $GP_B$  ( $fr_B$ ) and  $GP_G$  ( $fr_G$ ). Slopes calculated from the regression lines (solid lines) are significantly different from zero ( $P > 0.001$ ). Dashed lines correspond to the 95% confidence interval. Error bars indicate standard deviations of the histogram fittings.



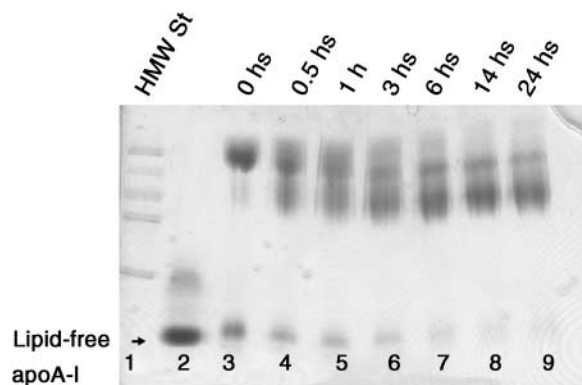


**Fig. 5.** Native 8–25% polyacrylamide gradient gel electrophoresis of the apoA-I exposed to DMPC/DSPC small unilamellar vesicles (SUVs) at 28°C and a weight ratio of 2.5:1 (lipid-protein). Lane 1 shows high molecular mass markers (HMW St; Amersham Pharmacia). Lane 2 shows control apoA-I incubated for 14 h in the absence of liposomes. Lanes 3–10 show the products of the rearrangement after the incubation periods shown at the top of each lane.

forming a complex of high molecular mass. The gradient of polyacrylamide used for this experiment (8–25%) did not allow us to determine whether this was a product of recombination of apoA-I into a lipid particle with a defined stoichiometry. Some apoA-I remained as lipid-free protein. A few minutes later (~30 min), the rearrangement of the protein into a complex, with an approximate molecular mass of 230 kDa, could be detected. As long as the incubation time increased, this complex tended to predominate. The size of this product is similar to that of reconstituted particles obtained by the sodium cholate method (34), in which each particle of 96 Å diameter contains two apoA-I molecules and the amphipathic  $\alpha$  helices of the protein are saturated with the lipids of the particle. In our hands, the efficiency of the rearrangement varied slightly from one experiment to another. This probably could be attributed to small differences in lipid-protein ratios, incubation temperature, or the efficiency of the sonication procedure.

To determine the final composition of the recombination product, we made SUVs containing DMPC/DSPC at a molar ratio of 0.7, incubated with apoA-I for 0.5, 3, 6, and 24 h, isolated the product, and quantified as described above. The composition of the complexes was almost the same for the first 6 h of incubation. The average molar composition was 46:49:1 DMPC/DSPC/apoA-I, which indicates a DMPC/DSPC molar ratio of  $0.93 \pm 0.04$ . However, particles isolated at 24 h showed a lower molar ratio (0.8), closer to the one present at the liposomes. We repeated the experiment with SUVs containing different starting DMPC/DSPC molar ratios (0.7–1.3). The composition of the isolated complexes was enriched in every case, in DMPC by 11–25% of the original liposomes (data not shown).

## DISCUSSION

The classic theory of the fluid mosaic model (35), in which lipids in biological membranes are organized in a

homogenous fluid-phase state, has evolved to a more dynamic concept of a heterogeneous arrangement of the complex mixture of lipids present in the membranes of cells. This heterogeneity could modulate the preferential partitioning of proteins and solutes as well as signaling and diffusion events (36, 37). For example, detergent-resistant lipid rafts are proposed to be naturally occurring lipid aggregates, rich in glycosphingolipids and cholesterol (38), regulating protein interactions. Domains with these characteristics, visualized in liposomes made of artificial lipid mixtures and with lipids extracted from brush border membranes, behaved as liquid-like domains but showed slower diffusion kinetics (39). It is plausible that the physiological conditions found in cells provide an environment in which domain formation and growth is triggered by small changes in lipid composition. The existence of these domains in the membranes can modify or, more importantly, regulate the lipid-protein interaction. It was also shown that the affinity of apoA-I for artificial PL bilayers (40, 41) is dependent on the lipid composition, and it was suggested that a special lipid microenvironment is required for apoA-I docking to the cell surface (42). Our GP kinetics experiment suggests that apoA-I removes lipids preferentially from the liquid-crystalline phase. We found (Fig. 4) that the composition of the coexisting domains did not change considerably during the experiment (the average GP value of each fraction remained unchanged during the experiment), but the fraction of the domains in the liquid state decreased. This fact reaffirms the notion that there is a preferential interaction of apoA-I with some liquid regions from which apoA-I removes lipids with a specific composition.

We attempted to characterize the products of the reaction between apoA-I and the mixed DMPC/DSPC SUVs. The results showed that, at short intervals, the protein extracts both lipids, but the liquid component is preferentially removed. However, the relative amount of DSPC we quantified in this case was higher than the amount estimated to be removed from the SUVs. This apparent discrepancy could be explained as follows. The reaction of apoA-I at the measured conditions with SUVs is very fast, as shown in Fig. 5. Almost all of the added apoA-I is combined in a few minutes, being less than 20% lipid free after 30 min of incubation (Fig. 5, lane 4). From the analysis of the isolated complexes, we did not find a significant difference in composition from 0.5 to 6 h of incubation, suggesting that we detected the final product even at the shortest tested time. On the other hand, as we mentioned above, the reaction of apoA-I with the SUV is very slow and is not complete during the 5 h that we followed the kinetics of interaction. Thus, we propose that at the initial steps (which we detected with SUVs), apoA-I forms lipidated products rich in the liquid component. After some time during which these products are present in the incubation cell, some PL transfer occurs back and forth within the vesicles (43) and the composition of the apoA-I complexes tends to be similar to that of the original liposomes. Using the same lipid components studied here, Swaney (44) found that the particle composition in the isolated

complexes is the same as in the initial mixture present at the liposomes. We observed the same phenomena at longer time periods. It is plausible that, under those time conditions (40 h in Swaney's experiments and 20 h in this work), PLs tend to reach an equilibrium attributable to the passive diffusion of the PLs within the remaining liposomes and the recently formed lipid complexes.

Another feature analyzed here is the temperature dependence of this reaction. Swaney (19) reported previously that micellization of MLVs made with the lipid mixture used here by apoA-I has its maximal rate at the onset temperature for DMPC melting (i.e., 28°C) (17). A fast kinetics of rearrangement was observed in our SUV experiments at the same temperature. By detecting the reaction through the decrease in light scattering, we confirmed that the micellization rate decreased abruptly when the reaction mixture was heated above 32°C or cooled below 25°C (Fig. 6). Instead, as can be deduced from Fig. 3, the kinetics of lipid removal from GUVs was so much slower, with as much as 40% of the lipids remaining at the vesicles after 5 h of incubation. We attribute this apparent discrepancy to the experimental procedure. On the one hand, the higher curvature of SUVs could make the reaction more efficient. On the other hand, protein diffusion in a nonstirred medium is necessary to reach the GUV surface, and we previously observed that apoA-I binding to POPC GUVs takes more than 30 min (14).

It is well known that any lipid phase diagram is dependent on the way lipids are organized (45). For example, according to the DSC phase diagram presented by Leidy et al. (18) using large unilamellar vesicles, this mixture should be in the solid state at 28°C, because the gel-to-gel/fluid transition occurs near 32–33°C. They suggested that at two special temperatures (31°C and 44°C) there is a maximum coexistence of DMPC-rich and DSPC-rich domains and that these form a dynamic structure of gel-fluid coexisting phases. It is possible that the effect that Leidy et al. (18) observed at 31°C in large unilamellar vesicles corresponds to the effect observed by Swaney (19) working

with MLVs at 28°C. Although using another probe, Bagatolli and Gratton (25) found that in DMPC/DSPC GUVs the fluid domains disappear at just under 28°C. Considering that all of these systems present some hysteresis (i.e., some differences between cooling and warming scans), it can be stated that by cooling to 28°C we are also just at the onset temperature for DSPC melting.

To further characterize the lipid distribution in GUVs under our particular working conditions, we looked at the top surface of GUVs and followed their morphology dependence on temperature. A clear domain separation was observed between ~55°C and 30°C. However, as the temperature cools down a few more degrees, not only does a vesicle deformation occur but the limit of each domain is more difficult to visualize (Fig. 1A, panel 4). This observation could be compatible with the disappearance of the lipid coexistence attributable to the solubilization of lipids. Another possibility is that when temperature decreases near the low phase boundary (~28°C), the diameter of the fluid domains decreases, and if their size is smaller than the pixel (0.52 µm) (22), we are unable to visualize their limit separately. Using different spectroscopic techniques, there is evidence of domain formation at the nanometer range (46–48) that is more dynamic in nature (49). If such small domains are present, the area of defects at the interphase between the solid and liquid-crystalline domains is maximum. It is probable that a particular condition of high stress occurs at the lipid bilayer in a small range of temperatures, in which a large area of surface defects (caused by small domain coexistence) favors lipid-protein interactions.


For example, ripple domains (in the nanometer range) were described for this particular mixture at temperatures similar to those studied here (50). The equilibrium between lipid phases creates special stress in the vesicle structure. For example, Bagatolli and Gratton (22) observed that giant vesicles composed of DMPC at temperatures corresponding or close to  $T_m$  suffer volume and shape changes independent of the scan rate. They attributed this defor-

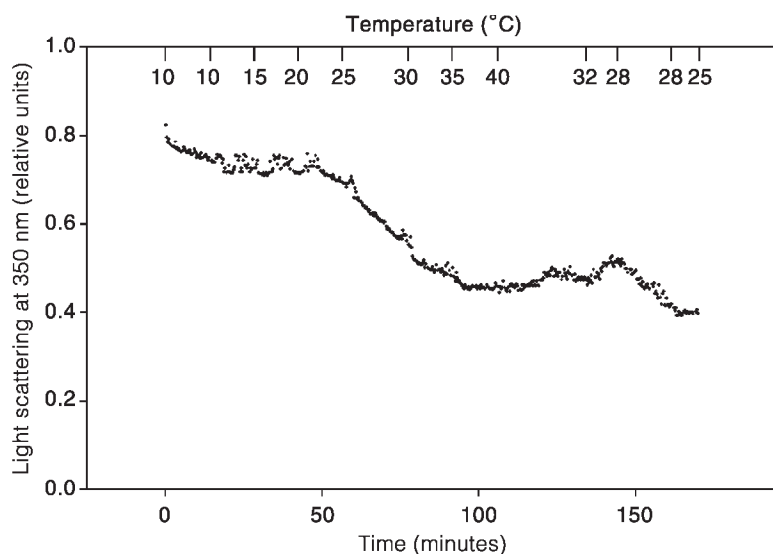


**Fig. 6.** Temperature dependence of the reaction of apoA-I with SUVs of DMPC/DSPC (1:1 molar ratio). SUVs were mixed with apoA-I as described in Materials and Methods and incubated for a few minutes at 10°C. Temperature (indicated at the top) was slowly increased (~0.3°C/min) to 40°C. An almost constant signal of light scattering was observed while the sample was warmed to ~26°C. However, a significant decrease in scattering was detected when the temperature was between 26°C and 31°C, indicating the formation of smaller products. The reaction stopped when the temperature was greater than 31°C, and no change in scattering was detected to 40°C. Then, the sample was cooled again to 28°C. A decrease in scattering was observed while the temperature was maintained at 28°C, but the reaction stopped if the sample was further cooled to 25°C.



mation to the predominance of gel domains that introduce stress in the lipid bilayer and suggested that defects present at the phase transition between the fluid and gel domains would allow water to flow through the membrane. They stated that gel-phase regions of the lipid bilayer become planar and that the vesicle bends along fluid line defects formed by the liquid-crystalline domains. In a different approach, Clerc and Thompson (51) observed that the permeation of small molecules across a two-component bilayer membrane exhibits a maximum when gel and liquid-crystalline phases coexist. They also determined that permeability is dependent on the lipid composition. They suggested that solute efflux kinetics is attributable to a particular structure of the bilayer, existing lateral density fluctuations at the domain interface that increase the probability of defect formation, and the average free volume in the acyl chain region (51).

We conclude that apoA-I interaction is maximum with liquid domains, from which protein removes lipids. However, to interact with these domains, special membrane conditions are required, probably a large area of defects produced by the boundaries of coexisting domains. 

The authors gratefully acknowledge Laura Hernandez for her expert technical assistance and the Banco de Sangre del Instituto de Hemoterapia de la Provincia de Buenos Aires (Argentina). The authors also thank Julia K. Wright for revising the English grammar. M.A.T. and H.A.G. are members of the Carrera del Investigador Científico, Consejo Nacional de Investigaciones Científicas y Tecnológicas, Argentina. This work was supported by grants from Agencia Nacional de Promoción Científica (BID 1201/OC-AR, PICT 01-08645) to H.A.G., by Fundación Antorchas, Argentina Grant 14022/124 to M.A.T., and by National Institutes of Health Grant RR-03155 to S.A.S., E.G., and T.L.H.

## REFERENCES

1. Miller, G. J., and N. E. Miller. 1975. Plasma-high-density-lipoprotein concentration and development of ischaemic heart-disease. *Lancet*. **1**: 16–19.
2. Rader, D. J. 2003. Regulation of reverse cholesterol transport and clinical implications. *Am. J. Cardiol*. **92**: 42–49.
3. Calabresi, L., M. Gomaschi, and G. Franceschini. 2003. Endothelial protection by high-density lipoproteins: from bench to bedside. *Arterioscler. Thromb. Vasc. Biol.* **23**: 1724–1731.
4. Cuchel, M., and D. J. Rader. 2003. Genetics of increased HDL cholesterol levels: insights into the relationship between HDL metabolism and atherosclerosis. *Arterioscler. Thromb. Vasc. Biol.* **23**: 1710–1712.
5. Mackness, M. I., and P. N. Durrington. 1995. HDL, its enzymes and its potential to influence lipid peroxidation. *Atherosclerosis*. **115**: 243–253.
6. Cockerill, G. W., and S. Reed. 1999. High-density lipoprotein: multipotent effects on cells of the vasculature. *Int. Rev. Cytol.* **188**: 257–297.
7. Kellner-Weibel, G., S. J. Luke, and G. H. Rothblat. 2003. Cytotoxic cellular cholesterol is selectively removed by apoA-I via ABCA1. *Atherosclerosis*. **171**: 235–243.
8. Fielding, C. J., and P. E. Fielding. 1995. Molecular physiology of reverse cholesterol transport. *J. Lipid Res.* **36**: 211–228.
9. Francone, O. L., P. V. Subbiah, A. van Tol, L. Royer, and M. Haghpassand. 2003. Abnormal phospholipid composition impairs HDL biogenesis and maturation in mice lacking Abca1. *Biochemistry*. **42**: 8569–8578.
10. Ji, Y., B. Jian, N. Wang, Y. Sun, M. de la Llera Moya, M. C. Phillips, G. H. Rothblat, J. B. Swaney, and A. R. Tall. 1997. Scavenger receptor BI promotes high density lipoprotein-mediated cellular cholesterol efflux. *J. Biol. Chem.* **272**: 20982–20985.
11. Fielding, C. J., and P. E. Fielding. 2001. Cellular cholesterol efflux. *Biochim. Biophys. Acta*. **1533**: 175–189.
12. Yokoyama, S. 2000. Release of cellular cholesterol: molecular mechanism for cholesterol homeostasis in cells and in the body. *Biochim. Biophys. Acta*. **1529**: 231–244.
13. Yancey, P. G., A. E. Bortnick, G. Kellner-Weibel, M. de la Llera Moya, M. C. Phillips, and G. H. Rothblat. 2003. Importance of different pathways of cellular cholesterol efflux. *Arterioscler. Thromb. Vasc. Biol.* **23**: 712–719.
14. Tricerri, M. A., S. A. Sanchez, C. Arnulphi, D. M. Durbin, E. Gratton, and A. Jonas. 2002. Interaction of apolipoprotein A-I in three different conformations with palmitoyl oleoyl phosphatidylcholine vesicles. *J. Lipid Res.* **43**: 187–197.
15. Massey, J. B., A. M. J. Gotto, and H. J. Pownall. 1981. Thermodynamics of lipid-protein interactions: interaction of apolipoprotein A-II from human plasma high-density lipoproteins with dimyristoylphosphatidylcholine. *Biochemistry*. **20**: 1575–1578.
16. Massey, J. B., A. M. J. Gotto, and H. J. Pownall. 1980. Dynamics of lipid-protein interactions. Interaction of apolipoprotein A-II from human plasma high density lipoproteins with dimyristoylphosphatidylcholine. *J. Biol. Chem.* **255**: 10167–10173.
17. Mabrey, S., and J. M. Sturtevant. 1976. Investigation of phase transitions of lipids and lipid mixtures by sensitivity differential scanning calorimetry. *Proc. Natl. Acad. Sci. USA*. **73**: 3862–3866.
18. Leidy, C., W. F. Wolters, K. Jorgensen, O. G. Mouritsen, and J. H. Crowe. 2001. Lateral organization and domain formation in a two-component lipid membrane system, using fluorescence resonance energy transfer (FRET), differential scanning calorimetry (DSC) and Fourier transform infrared resonance (FTIR). *Biophys. J.* **80**: 1819–1828.
19. Swaney, J. B. 1980. Mechanisms of protein-lipid interaction. *J. Biol. Chem.* **255**: 8791–8797.
20. Leroy, A., and A. Jonas. 1994. Native-like structure and self-association behavior of apolipoprotein A-I in a water/n-propanol solution. *Biochim. Biophys. Acta*. **1212**: 285–294.
21. Tricerri, M. A., H. A. Garda, and R. R. Brenner. 1994. A rapid and efficient procedure for the purification of human apolipoprotein A-I by using gel filtration HPLC. *Int. J. Biochromatogr.* **1**: 159–166.
22. Bagatolli, L. A., and E. Gratton. 1999. Two-photon fluorescence microscopy observation of shape changes at the phase transition in phospholipid giant unilamellar vesicles. *Biophys. J.* **77**: 2090–2101.
23. Dimitrov, D. S., and M. J. Angelova. 1987. Lipid swelling and liposome formation on solid surfaces in external electric fields. *Prog. Colloid Polym. Sci.* **73**: 48–56.
24. Sanchez, S. A., L. A. Bagatolli, E. Gratton, and T. L. Hazlet. 2002. A two-photon view of an enzyme at work: *Crotalus atrox* venom PLA2 interaction with single-lipid and mixed-lipid giant unilamellar vesicles. *Biophys. J.* **82**: 2232–2243.
25. Bagatolli, L. A., and E. Gratton. 2000. A correlation between lipid domain shape and binary phospholipid mixture composition in free standing bilayers: a two-photon fluorescence microscopy study. *Biophys. J.* **79**: 434–447.
26. Bagatolli, L. A., and E. Gratton. 2000. Two photon fluorescence microscopy of coexisting lipid domains in giant unilamellar vesicles of binary phospholipid mixtures. *Biophys. J.* **78**: 290–305.
27. Parasassi, T., M. Loiero, M. Raimondi, G. Ravagnan, and E. Gratton. 1993. Absence of lipid gel-phase domains in seven mammalian cell lines and in four primary cell types. *Biochim. Biophys. Acta*. **1153**: 143–154.
28. Chong, P. L., and P. T. Wong. 1993. Interactions of Laurdan with phosphatidylcholine liposomes: a high pressure FTIR study. *Biochim. Biophys. Acta*. **1149**: 260–266.
29. Parasassi, T., E. Gratton, W. Yu, P. Wilson, and M. Levi. 1997. Two photon fluorescence microscopy of LAURDAN generalized polarization domains in model and natural membranes. *Biophys. J.* **72**: 2413–2429.
30. Parasassi, T., G. De Stasio, G. Ravagnan, R. M. Rush, and E. Gratton. 1991. Quantitation of lipid phases in phospholipid vesicles by the generalized polarization of LAURDAN fluorescence. *Biophys. J.* **60**: 179–189.
31. Ibdah, J. A., and M. C. Phillips. 1988. Effect of lipid composition and packing on the adsorption of apolipoprotein A-I to lipid monolayers. *Biochemistry*. **27**: 7155–7162.

32. Folch, J., M. Lees, and G. H. Sloane-Stanley. 1957. A simple method for the isolation and purification of total lipids from animal tissues. *J. Biol. Chem.* **226**: 497–509.
33. Brenner, R. R., A. M. Bernasconi, M. S. Gonzalez, and O. J. Rimoldi. 2002. Dietary cholesterol modulates delta6 and delta9 desaturase mRNAs and enzymatic activity in rats fed a low-eFA diet. *Lipids*. **37**: 375–383.
34. Jonas, A. 1986. Reconstitution of high-density lipoproteins. *Methods Enzymol.* **128**: 553–582.
35. Singer, S. J., and G. L. Nicolson. 1972. The fluid mosaic model of the structure of cell membranes. *Science*. **175**: 720–731.
36. Golantsova, N. E., E. E. Gorbunova, and E. R. Mackow. 2004. Discrete domains within the rotavirus VP5\* direct peripheral membrane association and membrane permeability. *J. Virol.* **78**: 2037–2044.
37. Matko, J., A. Bodnar, G. Vereb, L. Bene, G. Vamosi, G. Szentesi, J. Szollosi, R. Gaspar, V. Horejsi, T. A. Waldmann, and S. Damjanovich. 2002. GPI-microdomains (membrane rafts) and signaling of the multi-chain interleukin-2 receptor in human lymphoma/leukemia T cell lines. *Eur. J. Biochem.* **269**: 1199–1208.
38. Fielding, C. J., and P. E. Fielding. 2003. Relationship between cholesterol trafficking and signaling in rafts and caveolae. *Biochim. Biophys. Acta*. **1610**: 219–228.
39. Dietrich, C., L. A. Bagatolli, Z. N. Volovyk, N. L. Thompson, M. Levi, K. Jacobson, and E. Gratton. 2001. Lipid rafts reconstituted in model membranes. *Biophys. J.* **80**: 1417–1428.
40. Yokoyama, S., D. Fukushima, J. P. Kupferberg, F. J. Kezdy, and E. T. Kaiser. 1980. The mechanism of activation of lecithin:cholesterol acyltransferase by apolipoprotein A-I and an amphiphilic peptide. *J. Biol. Chem.* **255**: 7333–7339.
41. Arnulphi, C., L. Jin, M. A. Tricerri, and A. Jonas. 2004. Enthalpy-driven apoA-I and lipid bilayer interaction indicating protein penetration upon lipid binding. *Biochemistry*. **43**: 12258–12264.
42. Chambenoit, O., Y. Hamon, D. Marguet, H. Rigneault, M. Rosse-neu, and G. Chimini. 2001. Specific docking of apolipoprotein A-I at the cell surface requires a functional ABCA1 transporter. *J. Biol. Chem.* **276**: 9955–9960.
43. Jonas, A., and G. T. Maine. 1979. Kinetics and mechanism of phosphatidylcholine and cholesterol exchange between single bilayer vesicles and bovine serum high-density lipoprotein. *Biochemistry*. **18**: 1722–1728.
44. Swaney, J. B. 1980. Properties of lipid-apolipoprotein association products. *J. Biol. Chem.* **255**: 8798–8803.
45. Mason, J. T. 1998. Investigation of phase transitions in bilayer membranes. *Methods Enzymol.* **295**: 468–494.
46. Bacia, K., D. Scherfeld, N. Kahya, and P. Schwille. 2004. Fluorescence correlation spectroscopy relates rafts in model and native membranes. *Biophys. J.* **87**: 1034–1043.
47. Silvius, J. R. 2003. Fluorescence energy transfer reveals microdomain formation at physiological temperatures in lipid mixtures modeling the outer leaflet of the plasma membrane. *Biophys. J.* **85**: 1034–1045.
48. Schram, V., H. N. Lin, and T. E. Thompson. 1996. Topology of gel-phase domains and lipid mixing properties in phase-separated two-component phosphatidylcholine bilayers. *Biophys. J.* **71**: 1811–1822.
49. Mouritsen, O. G., and K. Jorgensen. 1994. Dynamical order and disorder in lipid bilayers. *Chem. Phys. Lipids*. **73**: 3–25.
50. Kaasgaard, T., C. Leidy, J. H. Crowe, O. G. Mouritsen, and K. Jørgensen. 2003. Temperature-controlled structure and kinetics of ripple phases in one- and two-component supported lipid bilayers. *Biophys. J.* **85**: 350–360.
51. Clerc, S. G., and T. E. Thompson. 1995. Permeability of dimyristoyl phosphatidylcholine/dipalmitoyl phosphatidylcholine bilayer membranes with coexisting gel and liquid-crystalline phases. *Biophys. J.* **68**: 2333–2341.